

## Supporting information for:

# On the Emission Pattern of Nanoscopic Emitters in Planar Anisotropic Matrix and Nanoantenna Structures

Pu Zhang<sup>1</sup>, Peng-Long Ren<sup>1</sup>, and Xue-Wen Chen<sup>1\*</sup>

<sup>1</sup>School of Physics, Huazhong University of Science and Technology, Luoyu Road 1037, Wuhan, 430074, People's Republic of China

\*Email: [xuwen\\_chen@hust.edu.cn](mailto:xuwen_chen@hust.edu.cn)

In the following Supporting Information, we provide additional information for better understanding of the article, including the derivation of a key equation in the theory, the validation of the AnisoNFFT package, extended studies on emission pattern for various parameters, and the dependence of Purcell factor on emitter position in the matrix.

### 1. Derivation of Eq. (3) in the main text

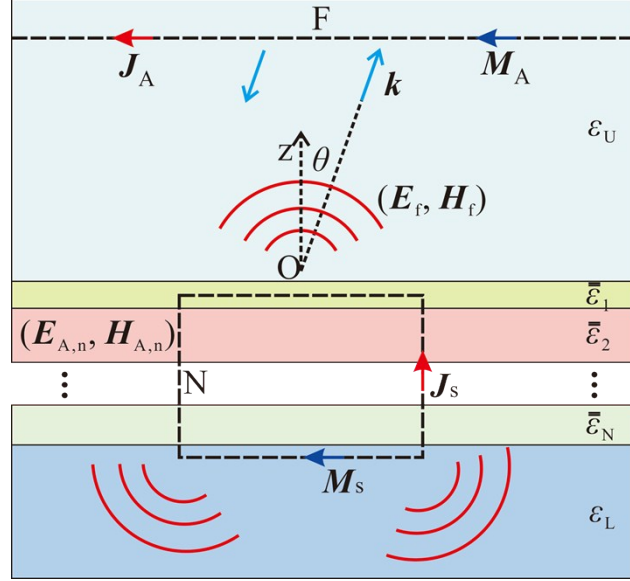


Fig. S1. Equivalent and auxiliary surface currents and their corresponding electromagnetic fields are illustrated in the planar multilayer system.

We start with Eq. (2) in the main text

$$\iint_N (E_{A,n} \cdot J_s - H_{A,n} \cdot M_s) dS = \iint_F (E_f \cdot J_A - H_f \cdot M_A) dS$$

The emission from the equivalent surface currents  $J_s$  and  $M_s$  as shown in Fig. S1 is expanded into plane waves (s-polarization)

$$E_f = \iint A_s(k) (k_t \times \hat{z}) e^{-ik \cdot r} dk_x dk_y$$

$$H_f = \iint A_s(k) \frac{k \times (k_t \times \hat{z})}{Z_U} e^{-ik \cdot r} dk_x dk_y$$

The auxiliary surface currents are assumed to generate an incident plane wave with wave vector  $k'$ ,

$$E_{A,i} = (k'_t \times \hat{z}) e^{ik' \cdot r}$$

$$H_{A,i} = \frac{(\mathbf{k}'_t \times \hat{\mathbf{z}}) \times \mathbf{k}'_t}{Z_U} e^{i\mathbf{k}' \cdot \mathbf{r}}$$

The auxiliary surface currents then are

$$J_A = -\hat{\mathbf{z}} \times H_{A,i}|_{z=z_0} = \frac{\hat{\mathbf{z}} \times \mathbf{k}'_t}{Z_U} \cos\theta' e^{i(\mathbf{k}'_t \cdot \mathbf{r}_t + k'_z z_0)}$$

$$M_A = \hat{\mathbf{z}} \times E_{A,i}|_{z=z_0} = \mathbf{k}'_t e^{i(\mathbf{k}'_t \cdot \mathbf{r}_t + k'_z z_0)}$$

We substitute the above expressions into Lorentz reciprocity theorem:

$$\begin{aligned} LHS &= \iint_N [E_{A,n} \cdot (\hat{\mathbf{n}} \times H_n) - H_{A,n} \cdot (-\hat{\mathbf{n}} \times E_n)] dS = \iint_N [(H_n \times E_{A,n}) + (E_n \times H_{A,n})] \cdot dS \\ RHS &= \iint_F \left[ \iint A_s(\mathbf{k}) (\mathbf{k}_t \times \hat{\mathbf{z}}) e^{-i(\mathbf{k}_t \cdot \mathbf{r}_t + k_z z)} dk_x dk_y \cdot \frac{\hat{\mathbf{z}} \times \mathbf{k}'_t}{Z_U} \cos\theta' e^{i(\mathbf{k}'_t \cdot \mathbf{r}_t + k'_z z)} \right. \\ &\quad \left. - \iint A_s(\mathbf{k}) \frac{\mathbf{k} \times (\mathbf{k}_t \times \hat{\mathbf{z}})}{Z_U} e^{-i(\mathbf{k}_t \cdot \mathbf{r}_t + k_z z)} dk_x dk_y \cdot \mathbf{k}'_t e^{i(\mathbf{k}'_t \cdot \mathbf{r}_t + k'_z z)} \right] dS \\ &= \iint A_s(\mathbf{k}) dk_x dk_y e^{i(k'_z - k_z)z_0} \left[ (\mathbf{k}_t \times \hat{\mathbf{z}}) \cdot \frac{\hat{\mathbf{z}} \times \mathbf{k}'_t}{Z_U} \cos\theta' - \frac{\mathbf{k} \times (\mathbf{k}_t \times \hat{\mathbf{z}})}{Z_U} \cdot \mathbf{k}'_t \right] \iint_{z=z_0} e^{i(\mathbf{k}'_t - \mathbf{k}_t) \cdot \mathbf{r}_t} dS \end{aligned}$$

The surface integral reduces to  $4\pi^2 \delta(k'_x - k_x) \delta(k'_y - k_y)$ , and we get

$$RHS = A_s(\mathbf{k}') \left[ (\mathbf{k}'_t \times \hat{\mathbf{z}}) \cdot \frac{\hat{\mathbf{z}} \times \mathbf{k}'_t}{Z_U} \cos\theta' - \frac{\mathbf{k}' \times (\mathbf{k}'_t \times \hat{\mathbf{z}})}{Z_U} \cdot \mathbf{k}'_t \right] 4\pi^2 = -\frac{8\pi^2}{Z_U} A_s(\mathbf{k}') \cos\theta'$$

Equating LHS and RHS leads to

$$A_s(\mathbf{k}) = -\frac{Z_U}{8\pi^2 \cos\theta} \iint_N [(H_n \times E_{A,n}) + (E_n \times H_{A,n})] \cdot dS$$

where we have dropped the prime for simplicity. We note that p-polarization can be derived in the same way.

## 2. Validation of the implementation

We have validated the package via two examples. The applicability of the implementation to the special case of isotropic multilayers is first tested with a simple scattering problem. A spherical silicon nanoparticle (with refractive index of 3.5 and radius of 285 nm) in free space is illuminated by a plane wave at the wavelength of 1500 nm. The polarization and wave vector are shown in Fig. S2(a). We view the nanoparticle as embedded in an air slab, so that the radiation pattern of the scattered field can be calculated with AnisoNFFT package. It is worthwhile to mention we have checked the convergence of the calculation. The radiation pattern converges with respect to the discretization number on the boundaries at about 200. Apart from the AnisoNFFT implementation, the accuracy also relies on the quality of the near field solutions. The radiation pattern was also made available from an NFFT method designed for isotropic media.<sup>1</sup> Good agreement between our results (red line) and those extracted from literature (grey dots) is illustrated in Fig. S2(b) and S2(c). Moreover the power scattered to the far field  $P_{\text{rf}}$  is found consistent with that obtained via integration of Poynting vector in the near field, confirming the correctness of our calculation from the energy conservation point of view.

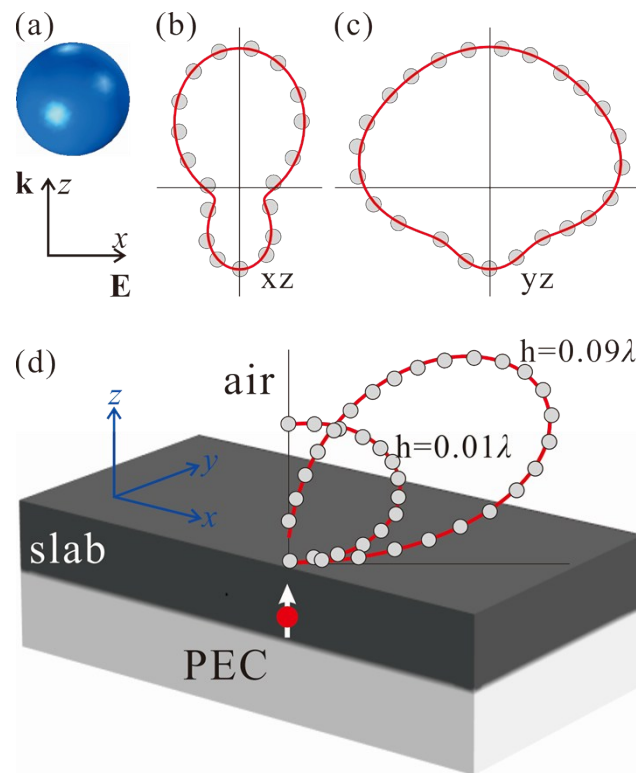


**Fig. S2** Validation of AnisoNFFT package. (a) A silicon nanoparticle of radius 285 nm is illuminated with a plane wave. The cross sections of the radiation pattern in xz-plane (b) and yz-plane (c) are compared between our results (solid red line) and data in literature (grey dots).<sup>1</sup> (d) Emission from a vertical dipole buried in an anisotropic slab of  $0.1\lambda$  thickness backed by a PEC ground. Cross sections of the radiation patterns are verified with results from Ref. 2.

The implementation is further verified with a microwave antenna problem. In the microwave engineering community sophisticated dyadic Green's function based NFFT methods have been developed for some antennas buried in anisotropic substrates.<sup>2</sup> Here we consider the radiation from a dipolar emitter situated inside a uniaxial slab ( $\epsilon_1=10.3\epsilon_0$  parallel to and  $\epsilon_2=13\epsilon_0$  perpendicular to the optic axis) backed by perfect electric conductor as shown in Fig. S2(d). The optic axis of the uniaxial medium is tilted off the z-axis by 60 degrees on the yz-plane. The thickness of the slab is  $0.1\lambda$  and the dipole is buried  $h=0.01\lambda$  or  $0.09\lambda$  below the top surface, where  $\lambda$  is the radiation wavelength. For both cases of dipole positions the p-polarized radiation patterns  $\sqrt{I_p}(\theta, \varphi)$  in the  $\varphi=60^\circ$  plane are presented in Fig. S2(d), where results from our calculation and Ref. 2 agree well.

### 3. Extended study on emission pattern of terrylene molecules in para- terphenyl

In the main text, we have shown terrylene molecules embedded at the center of a para-terphenyl matrix and coupled with a planar nanoantenna exhibit high directivity in the emission pattern when the matrix is 100 nm thick. Here we supplement the result with emission patterns with various geometrical and

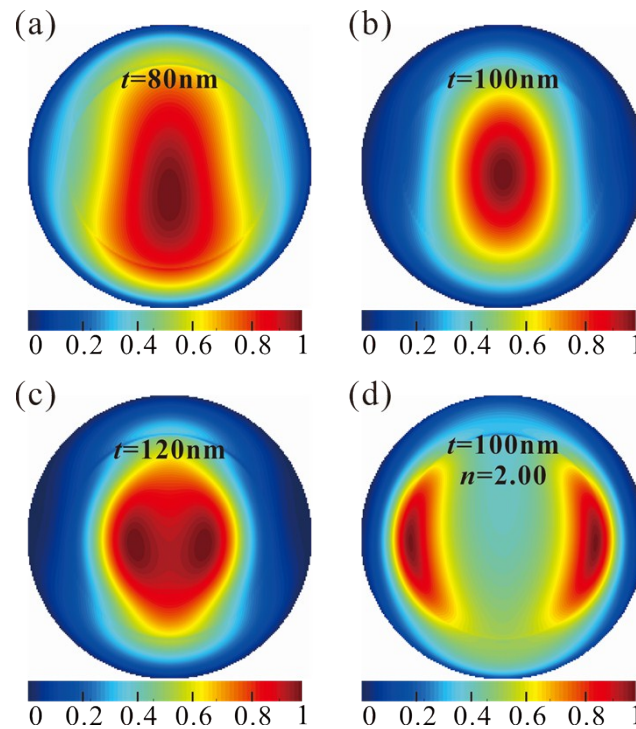


**Fig. S3.** The emission patterns from terrylene molecules embedded in a para-terphenyl matrix and coupled with a planar nanoantenna. (a)-(c) The BFP images for the matrix of thicknesses 80 nm, 100 nm and 120 nm; (d) The BFP image for the configuration with 100 nm thick matrix but isotropic approximation  $n = 2.0$ .

material parameters. The evolution of the emission pattern with matrix thickness is first studied. The BFP images for the configurations with a series of matrix thicknesses ( $t = 80$  nm, 100 nm, and 120 nm) are displayed in Fig. S3(a)-S3(c). At the thickness of 80 nm, the directivity deteriorates a bit with a distorted emission pattern. However, with a thicker matrix the emission pattern splits into two lobes and completely loses the beaming effect. We have approximated para-terphenyl as isotropic with a refractive index of 1.85 in the main text. However, based on the fact that the dipole moment of the emitter is largely perpendicular to the plane, one might like to take the  $z$  component 2.0 as an alternative choice for the approximated isotropic refractive index. Here we examine the emission pattern for this approximation and the BFP image for  $t = 100$  nm is demonstrated in Fig. S3(d). Compared with the anisotropic one (Fig. S3(b)) the emission pattern is seen to split into two widely separated lobes. The poor behavior could be explained by the larger deviation from the anisotropic refractive index in the average sense.

#### 4. Dependence of Purcell factor on emitter position

A silver half-cone dimer nanoantenna has been specially designed in the main text to boost the decay rate of defect emitters in an h-BN matrix. The emitter position relative to the nanoantenna is also an important factor in their interaction. In the h-BN matrix, the defects could occur randomly at different positions. The depth of the emitters below the top interface thus has decisive influence on the interaction with the nanoantenna and the absolute value of Purcell factor. For completeness, we studied the

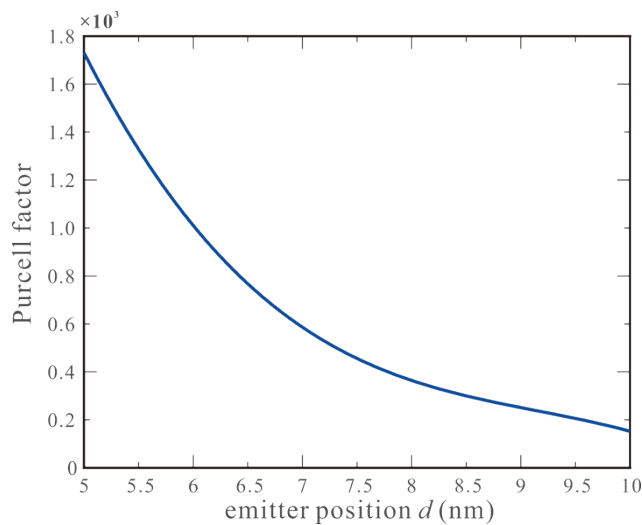


**Fig. S4.** The emission of defect emitters in an h-BN matrix at depth  $d$  below the top interface is enhanced by a silver half-cone dimer nanoantenna. The Purcell factor strongly depends on the emitter position  $d$ .

dependence of the Purcell factor on the emitter position and presented the result in Fig. S4. We see the Purcell factor varies from below 200 to about 1800 when the depth decreases from 10 nm to 5 nm, which tells us that the absolute value of the emission rate possibly measured in experiments would depend strongly on experimental conditions.

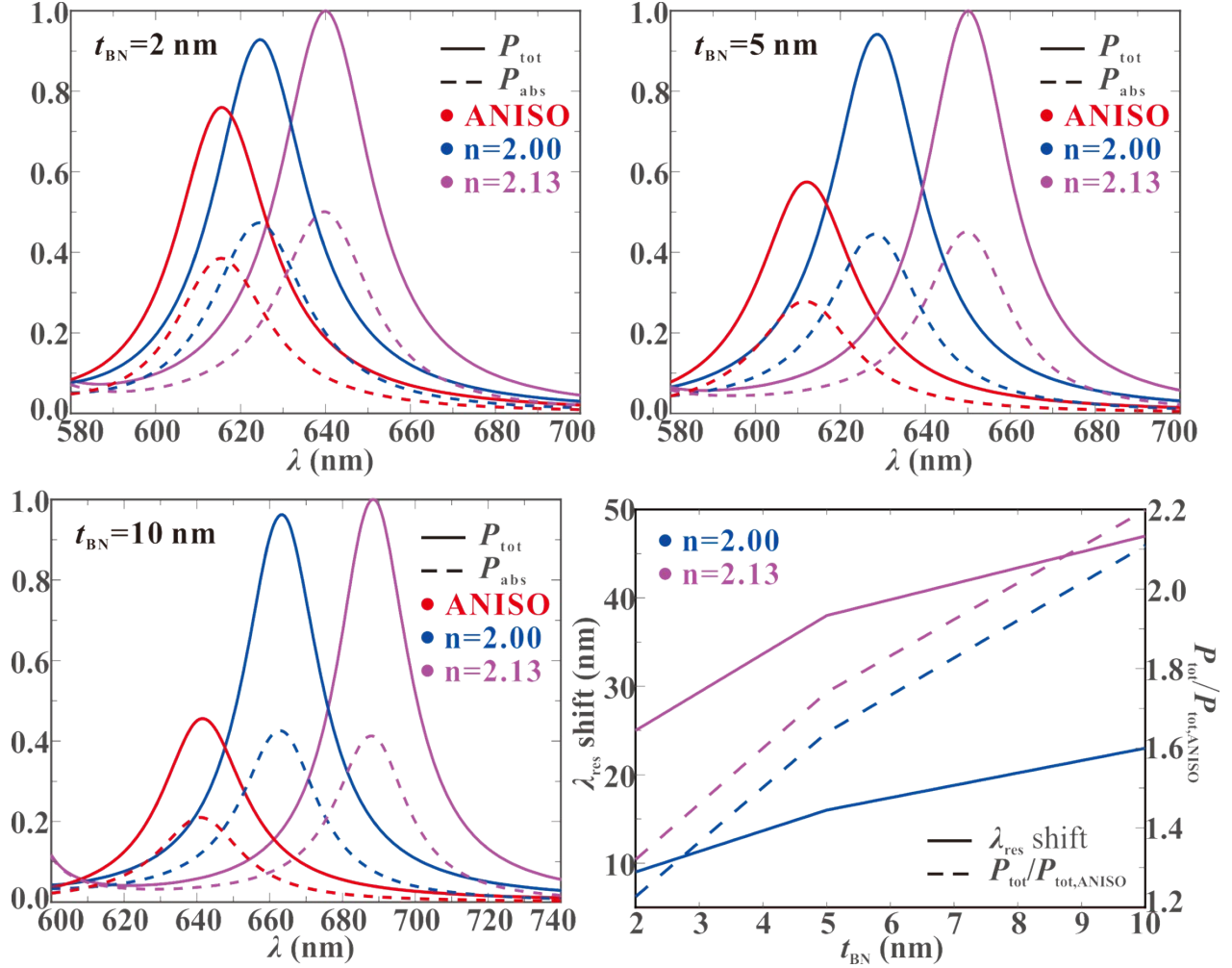


**Fig. S5.** The anisotropic effects of thin h-BN matrices ( $t_{BN} =$  (a) 2 nm, (b) 5 nm and (c) 10 nm) on total emission power (solid lines) and absorption (dashed lines). The curves in red, blue and purple represent the results with h-BN modeled by the birefringent refractive index,  $n = 2.00$  and  $n = 2.13$ , respectively. (d) The shift in resonance wavelengths relative to the anisotropic ones and the overestimation of total emission (normalized by the anisotropic values) are demonstrated as functions of thickness.

## 5. Anisotropic effects of few nanometer thick h-BN layers on emission

In the main text, we have assumed a 100 nm thick h-BN matrix hosting the single defect emitter. Defect emitters exist in various 2D materials and the matrix can be as thin as few nanometers, even down to

single atom layer. Here we scrutinize the anisotropic effects of few nanometer thick h-BN matrices ( $t_{\text{BN}} = 2 \text{ nm}, 5 \text{ nm}$  and  $10 \text{ nm}$ ) on photon emission. Specifically the thin h-BN matrix is considered in the same configuration as in Fig. 3(a) of the main text, except that the emitter is buried at the depth of half thickness. For the series of three thicknesses, the optical responses of the nanoantenna are characterized by total emission power  $P_{\text{tot}}$  and absorption  $P_{\text{abs}}$  (see Fig. S5(a)-S5(c)) with h-BN being modeled with birefringent refractive index or two isotropic approximations. It can be seen the isotropic approximations consistently redshift the resonance wavelengths  $\lambda_{\text{res}}$  and overestimate  $P_{\text{tot}}$ . In particular, the anisotropic effects, *i.e.* the shift in  $\lambda_{\text{res}}$  and the overestimation of the total emission ( $P_{\text{tot}}/P_{\text{tot,ANISO}}$ ), are still apparent even when the matrix is only few nanometer thick, as shown in Fig. S5(d). The extrapolation to the ultimate limit of one atom layer h-BN might be inaccurate due to the classical treatment, yet we believe anisotropic effects should be taken into account to obtain reliable prediction of photon emission properties.

## REFERENCES

- (1) J. Yang, J. P. Hugonin and P. Lalanne, *ACS Photonics*, 2016, **3**, 395-402.
- (2) A. Eroglu and J. K. Lee, *IEEE Trans. Antennas Propag.*, 2005, **53**, 3963-3973.